A POSTERIORI ERROR ESTIMATION FOR A CUT CELL FINITE VOLUME METHOD WITH UNCERTAIN INTERFACE LOCATION

J.B. Collins,[1] Don Estep,[2] & Simon Tavener[2,]*

[1]*Department of Mathematics, Chemistry, and Physics, West Texas A&M University, Canyon, TX 79016*

[2]*Department of Mathematics, Colorado State University, Fort Collins, CO 80523*

Original Manuscript Submitted: 08/18/2015; Final Draft Received: 08/18/2015

We study a simple diffusive process in which the diffusivity is discontinuous across an interface interior to the domain. In many situations, the location of the interface is measured at a small number of locations and these measurements contain error. Thus the location of the interface and the solution itself are subject to uncertainty. Further, the location of the interface may have a strong impact on the accuracy of the solution. A Monte Carlo approach is employed which requires solving a large number of sample problems, each with a different interface location. To solve these problems, a mixed finite element cut-cell method has been developed that does not require the mesh to conform to the interface. An efficient adjoint-based a posteriori *technique is used to estimate the error in a quantity of interest for each sample problem. This error has a component due to the numerical approximation of the diffusive process and a component arising from the uncertainty in the interface location. A recognition of these separate sources of error is necessary in order to construct effective adaptivity strategies.*

KEY WORDS: *Uncertainty Quantification, Stochastic modeling, Spatial uncertainty, Porous media flow*

1. INTRODUCTION

We address a commonly encountered situation in which a small number of experimental measurements are used to specify a continuous input function to a complex physical problem. These experimental measurements may define for example, the geometry, material properties, boundary conditions or forcing functions. Based on these uncertain data, we construct a stochastic model for the problem. A typical Monte Carlo approach assumes a probability distribution for the input function and draws random samples from this distribution. The physical problem is formulated for each random sample and solved by an appropriate numerical method, and a quantity of interest is calculated based on the numerical solution. Ignoring inadequacies in the model itself, the so-called "modeling error", uncertainty in the quantity of interest arises from both the error in the input function and from the error introduced by numerical approximation. These errors are not independent, since the numerical error will vary according to the value of the input function. A general framework for problems of this nature, including probabilistic bounds on the approximate cumulative distribution function for the quantity of interest is developed in [1]. It requires however, that a distinct adjoint problem be solved for each realization of the physical problem. The advantages to be accrued from identifying the error in large computational problems into components that arise from distinct sources has been previously recognized by several authors including [2], and more recently by [3] who use a sensitivity analysis to determine the relative sizes of each contribution.

Here, we consider the situation in which a well-defined deterministic physical problem exists, if only one were able to describe it with sufficient precision. In many situations this is impractical or impossible and the problem can

*Correspond to: Simon Tavener, E-mail: tavener@math.colostate.edu, URL: http://math.colostate.edu/tavener/

2152–5080/10/$35.00

only be formulated with uncertainty. We focus on situations in which the continuous input function prescribes the differential operator defining the problem rather than simply establishing a forcing function or boundary condition. To provide a specific context, we consider the diffusive process

$$\begin{aligned} -\nabla \cdot (a(\boldsymbol{x})\nabla p) &= f, \quad \text{in } \Omega, \\ p &= g, \quad \text{on } \partial\Omega, \end{aligned} \tag{1}$$

in a convex polyhedral domain $\Omega \in \mathbb{R}^2$ with boundary $\partial\Omega$ that consists of two distinct materials with different material properties separated by a smooth interface Γ interior to Ω, as shown in Fig. 1. We assume that the diffusivity $a(\boldsymbol{x})$ changes discontinuously across Γ but require that the solution be continuous and have continuous normal flux across Γ. Specifically, we assume that a is smooth in each subdomain of Ω determined by Γ, $a(\boldsymbol{x})$ has one-sided limits at Γ, and $a(\boldsymbol{x})$ is bounded below by a positive number. We also assume that $f \in L^2(\Omega)$ and $g \in H^{1/2}(\partial\Omega)$. Finally, we assume $p \in W = L^2(\Omega)$ and $\boldsymbol{u} = -a\nabla p \in \boldsymbol{V} = \mathrm{H}(\mathrm{div};\Omega) = \big(\boldsymbol{u} \in (L^2(\Omega))^2 : \mathrm{div}\, \boldsymbol{u} \in L^2(\Omega)\big)$. Such problems arise in many contexts, e.g. flow of oil reservoir through heterogenous porous media [4–6], the elastic [7–9] and thermal [10] properties of composite materials and the modeling of nuclear fuel rods [11–13].

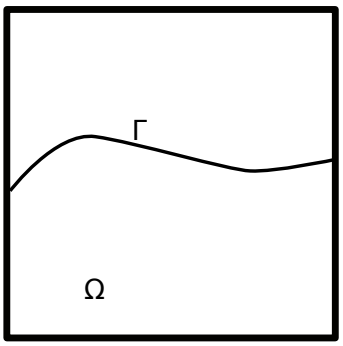

FIG. 1: The domain for the interface problems.

Locally conservative methods, and in particular finite volume methods, are popular in many application domains for diffusive and transport problems. Finite volume methods are generally easier to construct and implement on regularly-shaped discretizations, leading to "cut-cell" techniques in which an interface cuts through the discretization cells. In previous work [14], we developed a cut-cell finite element method, the Mixed Finite Element Cut-Cell (MFEC) method that is equivalent to the Ghost Fluid Method in simple cases. We extend our earlier work to the situation in which the interface location is not known everywhere, but is identified by its location at a small number of points P, and further, the locations of these few points are not known precisely. To simplify matters, we assume that the definition of $a(\boldsymbol{x})$ is known exactly on either side of the interface, as well as other data such as the source and boundary terms. Therefore, the only uncertainty arises due to the location of the interface. However, the location of the interface strongly influences the accuracy of the solution. We refer to this problem as the *stochastic interface problem*.

We construct a penalized spline approximation [10, 15] to the interface location based on P measurements of the interface location. We then assume a given statistical model for the (independent) errors of these P measurements and construct N realizations of the interface, thereby defining N "sample" problems. The error in the quantity of interest for each sample problem is determined as the sum of the modeling and discretization errors associated with a "nominal" problem, and the error associated with the difference between the nominal problem and the sample problem. Both require the solution to an adjoint problem to define a generalized Green's function. (The role of the Green's function in uncertainty quantification for steady state flow in randomly heterogeneous porous media such problems has previously been recognized by [16, 17]. Efficient techniques for computing the Green's function in this context are developed in [18].) Our approach enables the dominant source of error in the quantity of interest to

be determined, which may be either the finite element discretization or the uncertainty in the measurements of the interface location. We demonstrate the accuracy of our *a posteriori* error estimate for a range of situations.

In Section 2 we define the interface problem and the construction of the interface based on a small number of experimental measurements. In Section 3 the Mixed Finite Element Cut-Cell method proposed in [14] is outlined. The error analyses for the nominal and sample problems are performed in Section 4. Numerical results are provided in Section 5 and our conclusions are presented in Section 6.

2. PROBLEM DESCRIPTION

We begin by stating the deterministic elliptic interface problem, in order to introduce notation used for the stochastic interface problem. The diffusion coefficient $a(\boldsymbol{x};\Gamma) : \Omega \to \mathbb{R}$ depends both on the spatial variable $\boldsymbol{x} \in \Omega$ and implicitly on the interface Γ which partitions the domain Ω into two connected subregions. The interface is defined as $\Gamma = \{\boldsymbol{x} : \gamma(\boldsymbol{x}) = 0\}$ for some function $\gamma : \Omega \to \mathbb{R}^3$. The diffusion coefficient is defined piecewise on either side of the interface as,

$$a(\boldsymbol{x};\Gamma) = \begin{cases} a_N(\boldsymbol{x}), & \gamma(\boldsymbol{x}) < 0, \\ a_P(\boldsymbol{x}), & \gamma(\boldsymbol{x}) > 0. \end{cases} \tag{2}$$

The deterministic elliptic interface problem is defined by

$$\begin{aligned} -\nabla \cdot (a(\boldsymbol{x})\nabla p) &= f, \quad \boldsymbol{x} \in \Omega \setminus \Gamma, \\ [p] &= 0, \quad \boldsymbol{x} \in \Gamma, \\ [a(\boldsymbol{x})\nabla p \cdot \boldsymbol{n}] &= 0, \quad \boldsymbol{x} \in \Gamma, \\ p &= g, \quad \boldsymbol{x} \in \partial\Omega, \end{aligned} \tag{3}$$

for some source term f and boundary conditions g. Note that the state variable p and the flux $a(\boldsymbol{x})\nabla p \cdot \boldsymbol{n}$ are continuous across the interface. This assumption is made throughout the paper and so these conditions are not explicitly stated below.

2.1 Spline approximation to the interface

In most situations an interface will be known only through a finite number of measurements $(x_i, y_i)_{i=1}^P$ located along the interface. Furthermore, these measurements will be subject to error. To construct a spline interpolation we first introduce an approximate arclength parameter s_i, where

$$s_1 = 0, \quad s_i = s_{i-1} + \sqrt{(x_i - x_{i-1})^2 + (y_i - y_{i-1})^2}\,, \quad i = 2, \ldots, P,$$

to give $(x(s_i), y(s_i))_{i=1}^P$. We use penalized splines (P-Splines) [19] to approximate the functions $x(s)$ and $y(s)$ which define the interface.

The penalized spline method uses a model function $y = m(x;\boldsymbol{\beta})$. The parameters $\boldsymbol{\beta} \in \mathbb{R}^M$ are determined such that they minimize a least squares error term and a penalized regularity term given by

$$\sum_{i=1}^{P} [y_i - m(x_i;\boldsymbol{\beta})]^2 + \lambda D(m(x;\boldsymbol{\beta})). \tag{4}$$

The regularity function D can have many different forms, all of which aim to smooth the spline. The smoothing parameter λ determines the relative weighting of the least squares error and the regularization terms. Here

$$m(x;\boldsymbol{\beta}) = \beta_0 + \beta_1 x + \beta_2 x^2 + \beta_3 x^3 + \sum_{k=1}^{K} \beta_{3+k}(x - \kappa_k)_+^3\,, \tag{5}$$

where K is the number of knots in the spline, κ_k are the knot locations and D penalizes the parameters $\beta_{3+k}, k = 1, \ldots, K$. We therefore seek to minimize the function

$$\sum_{i=1}^{P} [y_i - m(x_i; \boldsymbol{\beta})]^2 + \lambda \sum_{k=1}^{K} \beta_{3+k}^2 \,. \tag{6}$$

The smoothing parameter λ is selected so as to minimize the Generalized Cross Validation (GCV) statistic, defined by

$$\text{GCV}(\lambda) = \frac{P^{-1} \sum_{i=1}^{P} [y_i - m(x_i; \hat{\boldsymbol{\beta}}(\lambda))]^2}{[1 - P^{-1} \text{tr}\, S(\lambda)]^2} \,, \tag{7}$$

where $S(\lambda) = X(X^T X + \lambda D)^{-1} X^T \in \mathbb{R}^{P \times P}$, $X \in \mathbb{R}^P$ is the vector with elements $x_i,\ i = 1, \ldots, P$ and $\hat{\boldsymbol{\beta}}(\lambda)$ is the vector of coefficients which minimize (6) for a particular λ. Let $\hat{\lambda}$ be the optimal smoothing parameter such that the GCV is minimized. We approximate $\hat{\lambda}$ by establishing a grid of 100 values of λ from 10^{-12} to 10^{12}, and choosing the value of lambda from that grid which yields the minimum value of the GCV [19].

The knots κ_k were uniformly spaced throughout the domain. We examined the number of changes in concavity in order to determine the number of knots need to reproduce the required shape. As a rule of thumb we chose one knot per change in concavity which works well for most shapes.

2.2 Sample problems

We now consider a random interface $\Gamma(Z)$ which is dependent upon a random variable Z. The diffusion coefficient corresponding to the random interface $\Gamma(Z)$ is

$$a(\boldsymbol{x}; \Gamma(Z)) = \begin{cases} a_N(\boldsymbol{x}), & \gamma(\boldsymbol{x}; Z) < 0, \\ a_P(\boldsymbol{x}), & \gamma(\boldsymbol{x}; Z) > 0. \end{cases} \tag{8}$$

The random interface $\Gamma(Z)$ represents uncertainty in our knowledge of the location of the interface. The stochastic interface problem is then given by

$$\begin{aligned} -\nabla \cdot (a(\boldsymbol{x}; \Gamma(Z)) \nabla p) &= f, \quad \boldsymbol{x} \in \Omega \setminus \Gamma(Z), \\ p &= g, \quad \boldsymbol{x} \in \partial\Omega. \end{aligned} \tag{9}$$

Given a set of measurements of the interface location, $(x_i^{(n)}, y_i^{(n)}),\ i = 1, \ldots, P$ we use P-Splines to construct an interface $\Gamma^{(n)}$, a sample from the distribution of interfaces $\Gamma(Z)$, and define the following sample interface problem,

$$\begin{cases} -\nabla \cdot \left(a^{(n)} \nabla p^{(n)} \right) = f, & \boldsymbol{x} \in \Omega \setminus \Gamma^{(n)}, \\ p^{(n)} = g, & \boldsymbol{x} \in \partial\Omega, \end{cases} \tag{10}$$

where $a^{(n)} = a(\boldsymbol{x}; \Gamma^{(n)})$.

2.3 The "nominal" problem

For the error representation formulae derived in §4, we require an approximation of the true interface. We construct the *nominal* interface $\bar{\Gamma}$ as the P-Spline whose coefficients are the mean of the coefficients of all sample interfaces. The nominal interface problem is

$$\begin{aligned} -\nabla \cdot (\bar{a} \nabla \bar{p}) &= f, \quad \boldsymbol{x} \in \Omega \setminus \bar{\Gamma}, \\ \bar{p} &= g, \quad \boldsymbol{x} \in \partial\Omega, \end{aligned} \tag{11}$$

where $\bar{a} = a(\boldsymbol{x}, \bar{\Gamma})$ is the nominal diffusivity coefficient.

3. THE MIXED FINITE ELEMENT CUT-CELL METHOD (MFEC)

The Mixed Finite Element Cut-Cell (MFEC) Method was developed in [14] and uses a fixed (rectangular) grid rather than a grid that is adapted to the interface. This leads to a "cut-cell" problem which is particularly appropriate for our current purposes since the finite-element grid is independent of the precise location of each realization (sample) of the interface.

3.1 Constructing the model problem

The MFEC method approximates the discontinuous diffusion coefficient a with a model problem having a continuous diffusion coefficient a_m. The model coefficient differs from a only within a modeling domain Ω_d, the boundary of which coincides with cell boundaries. Within the modeling domain, a_m is a continuous, positivity preserving interpolant defined according to Algorithm 3.1. The model problem is then solved using a mixed finite element method with specially chosen approximation and quadrature to produce a solution which is nodally equivalent to a cell-centered finite volume method.

Algorithm 3.1. **`[Constructing the model diffusivity coefficient`** a_m **`in`** Ω_d**`. ]`**

1: *The modeling domain* Ω_d. A "cut cell" is a cell that is either cut by the interface or a cell that is adjacent to a cell that is cut by the interface. The modeling domain is the union of all cut cells.
2: *Cell centers in* Ω_d. The value of a_m at the center of each cell in Ω_d is the average of a in that cell.
3: *Midpoints of cell boundaries.* The value of a_m at the midpoints of cell boundaries between two cells in Ω_d is set by one of two methods. If the interface lies between the two cell centers then a_m is the harmonic average of a at the two cell centers. Otherwise, a_m is the normal average of a at the two cell centers.
4: *Cell vertices.* Two diagonal lines, each connecting two cell centers pass through every vertex. The value of a_m at the cell vertex is the (normal) average two values that are calculated along each diagonal. The value assigned to each diagonal is either the harmonic or normal average of a at the two cell centers connected by the diagonal. The choice of averaging technique is the same as in Step 3. If the interface cuts the diagonal line connecting the cell centers, the harmonic average is used. Otherwise, the normal average is used.
5: *Remaining values.* The remaining values of a_m lie on the boundary of Ω_d. The value of a_m is set by evaluating a at these points.

Since a biquadratic interpolant can allow negative values in between the interpolation nodes, we use a positivity preserving, rational polynomial within Ω_d to interpolate the nodal values calculated via Algorithm 3.1 in order to ensure that the model coefficient is positive at all points within the domain.

3.2 The mixed finite element method

The model problem corresponding to the nominal problem (11) is

$$\begin{cases} -\nabla\cdot(\bar{a}_m\nabla\bar{p}_m) = f, & \boldsymbol{x}\in\Omega\setminus\bar{\Gamma}, \\ \bar{p}_m = g, & \boldsymbol{x}\in\partial\Omega. \end{cases} \tag{12}$$

In order to solve (12) using a mixed finite element method, we introduce an auxiliary variable $\bar{\boldsymbol{u}}_m = -\bar{a}_m\nabla\bar{p}_m$, and the function spaces

$$W = L^2(\Omega), \quad \boldsymbol{V} = H(\text{div};\Omega).$$

In weak form, equation (12) becomes: Find $(\bar{p}_m, \bar{\boldsymbol{u}}_m)\in W\times\boldsymbol{V}$ such that

$$\begin{aligned} (\bar{a}_m^{-1}\bar{\boldsymbol{u}}_m, \boldsymbol{v})_\Omega - (\bar{p}_m, \nabla\cdot\boldsymbol{v})_\Omega &= -\langle g, \boldsymbol{v}\cdot\boldsymbol{n}\rangle_{\partial\Omega} \quad \forall\,\boldsymbol{v}\in\boldsymbol{V}, \\ (\nabla\cdot\bar{\boldsymbol{u}}_m, w)_\Omega &= (f, w)_\Omega \quad \forall\, w\in W, \end{aligned} \tag{13}$$

where $(\cdot,\cdot)_\Omega$ and $\langle\cdot,\cdot\rangle_{\partial\Omega}$ represent the $L^2(\Omega)$ and $L^2(\partial\Omega)$ inner products respectively. We use the first-order Raviart-Thomas spaces, $W_h \subset W$ and $\boldsymbol{V}_h \subset \boldsymbol{V}$ [20, 21] and specific quadrature to produce a finite element scheme that is nodally equivalent with a cell-centered finite volume method [22].

The MFEC method for the model problem corresponding to the nominal problem (11) is: Find $(\bar{p}_{m,h}, \bar{\boldsymbol{u}}_{m,h}) \in W_h \times \boldsymbol{V}_h$ such that

$$\begin{aligned}(\bar{a}_m^{-1}\bar{\boldsymbol{u}}_{m,h}, \boldsymbol{v}_h)_{\Omega,Q} - (\bar{p}_{m,h}, \nabla\cdot\boldsymbol{v}_h)_\Omega &= -\langle g, \boldsymbol{v}_h\cdot\boldsymbol{n}\rangle_{\partial\Omega,M} \quad \forall\, \boldsymbol{v}_h \in \boldsymbol{V}_h,\\ (\nabla\cdot\bar{\boldsymbol{u}}_{m,h}, w_h)_\Omega &= (f, w_h)_{\Omega,M_xM_y} \quad \forall\, w_h \in W_h,\end{aligned} \tag{14}$$

where M is the midpoint rule, M_i, T_i represent the midpoint and trapezoid rule respectively in the ith coordinate direction, and

$$(\boldsymbol{v},\boldsymbol{w})_{\Omega,Q} = (\boldsymbol{v}_x,\boldsymbol{w}_x)_{\Omega,T_xM_y} + (\boldsymbol{v}_y,\boldsymbol{w}_y)_{\Omega,M_xT_y}, \tag{15}$$

where $\boldsymbol{v} = (\boldsymbol{v}_x,\boldsymbol{v}_y)^\top, \boldsymbol{w} = (\boldsymbol{w}_x,\boldsymbol{w}_y)^\top$.

Similarly, the MFEC method for the model problem corresponding to each sample interface problem (10) is: Find $\left(p_{m,h}^{(n)}, \boldsymbol{u}_{m,h}^{(n)}\right) \in W_h \times \boldsymbol{V}_h$ such that

$$\begin{aligned}\left(a_m^{(n)^{-1}}\boldsymbol{u}_{m,h}^{(n)}, \boldsymbol{v}_h\right)_{\Omega,Q} - \left(p_{m,h}^{(n)}, \nabla\cdot\boldsymbol{v}_h\right)_\Omega &= -\langle g, \boldsymbol{v}_h\cdot\boldsymbol{n}\rangle_{\partial\Omega,M} \quad \forall\, \boldsymbol{v}_h \in \boldsymbol{V}_h,\\ \left(\nabla\cdot\boldsymbol{u}_{m,h}^{(n)}, w_h\right)_\Omega &= (f, w_h)_{\Omega,M_xM_y} \quad \forall\, w_h \in W_h,\end{aligned} \tag{16}$$

where $a_m^{(n)}$ is the model diffusion coefficient associated with the sample diffusion coefficient $a^{(n)}$.

4. ADJOINT BASED *A POSTERIORI* ERROR ESTIMATION

Consider a linear quantity of interest, $\mathcal{Q}(p) = (p,\psi)_\Omega$ for some $\psi \in L^2(\Omega)$. Defining $e_p^{(n)} = \bar{p} - p_{m,h}^{(n)}$ to be the pointwise error, $\mathcal{Q}(e_p^{(n)}) = (e_p^{(n)},\psi)_\Omega$. Note that errors are defined relative to the exact solution of the nominal problem. We first derive an error estimate for the approximate solution to the nominal problem (11) and then obtain two estimates for the error for each sample problem (10).

4.1 Error estimation for the nominal interface problem

We begin by defining the adjoint to the nominal problem which is,

$$\begin{aligned}\bar{a}^{-1}\bar{\boldsymbol{\varphi}}_{\boldsymbol{u}} - \nabla\bar{\varphi}_p &= 0, \quad x\in\Omega\setminus\bar{\Gamma},\\ -\nabla\cdot\bar{\boldsymbol{\varphi}}_{\boldsymbol{u}} &= \psi, \quad x\in\Omega\setminus\bar{\Gamma},\\ \langle\bar{\varphi}_p, \boldsymbol{v}\cdot\boldsymbol{n}\rangle_{\partial\Omega} &= 0, \quad x\in\partial\Omega,\ \ \forall\,\boldsymbol{v}\in \mathrm{H(div};\Omega).\end{aligned} \tag{17}$$

This adjoint problem is used to determine the error representation formula for the nominal problem.

Theorem 4.1. **[Error estimate for the nominal interface problem]**
Let $(\bar{p},\bar{\boldsymbol{u}})$ and $(\bar{p}_{m,h},\bar{\boldsymbol{u}}_{m,h})$ satisfy (11) and (14) respectively. Also, let $(\bar{\varphi}_p,\bar{\boldsymbol{\varphi}}_{\boldsymbol{u}})$ satisfy (17). Defining the error to be $\bar{e}_p = \bar{p} - \bar{p}_{m,h}$, we have

$$\begin{aligned}(\bar{e}_p,\psi)_\Omega = \big(f, \bar{\varphi}_p - \mathbb{P}\bar{\varphi}_p\big)_\Omega - \langle g, (\bar{\boldsymbol{\varphi}}_{\boldsymbol{u}} - \pi\bar{\boldsymbol{\varphi}}_{\boldsymbol{u}})\cdot\boldsymbol{n}\rangle_{\partial\Omega} - (\bar{a}_m^{-1}\bar{\boldsymbol{u}}_{m,h}, \bar{\boldsymbol{\varphi}}_{\boldsymbol{u}} - \pi\bar{\boldsymbol{\varphi}}_{\boldsymbol{u}})_{\Omega,Q}\\ + QE1(\bar{\boldsymbol{\varphi}}_{\boldsymbol{u}}) + QE2(\pi\bar{\boldsymbol{\varphi}}_{\boldsymbol{u}}) + QE3(\mathbb{P}\bar{\varphi}_p)\\ + \left((\bar{a}_m^{-1} - \bar{a}^{-1})\bar{\boldsymbol{u}}_{m,h}, \bar{\boldsymbol{\varphi}}_{\boldsymbol{u}}\right)_{\Omega,Q},\end{aligned} \tag{18}$$

where

$$\begin{aligned}QE1(\boldsymbol{v}) &= (\bar{a}^{-1}\bar{\boldsymbol{u}}_{m,h},\boldsymbol{v})_{\Omega,Q} - (\bar{a}^{-1}\bar{\boldsymbol{u}}_{m,h},\boldsymbol{v})_\Omega,\\ QE2(\boldsymbol{v}) &= \langle g, \boldsymbol{v}\cdot\boldsymbol{n}\rangle_{\partial\Omega,M} - \langle g, \boldsymbol{v}\cdot\boldsymbol{n}\rangle_{\partial\Omega},\\ QE3(w) &= (f,w)_\Omega - (f,w)_{\Omega,M},\end{aligned} \tag{19}$$

and $\mathbb{P}$ and π are projections onto the finite element spaces W_h and $\boldsymbol{V}_h$ respectively.

Proof. The derivation of the error representation formula (18) is similar to the derivation in [14]. The difference is the order in which terms are added. For the proof, we define $\bar{e}_{\boldsymbol{u}} = \bar{\boldsymbol{u}} - \bar{\boldsymbol{u}}_{m,h}$. Then from (17) and integrating by parts,

$$\begin{aligned}
(\bar{e}_p, \psi)_\Omega &= -(\bar{e}_p, \nabla\cdot\bar{\boldsymbol{\varphi}}_{\boldsymbol{u}})_\Omega + (\bar{a}^{-1}\bar{e}_{\boldsymbol{u}}, \bar{\boldsymbol{\varphi}}_{\boldsymbol{u}})_\Omega + (\nabla\cdot\bar{e}_{\boldsymbol{u}}, \bar{\varphi}_p)_\Omega \qquad \text{[by (17)]} \\
&= (f, \bar{\varphi}_p)_\Omega - \langle g, \bar{\boldsymbol{\varphi}}_{\boldsymbol{u}}\cdot\boldsymbol{n}\rangle_{\partial\Omega} + (\bar{p}_{m,h}, \nabla\cdot\bar{\boldsymbol{\varphi}}_{\boldsymbol{u}})_\Omega - (\bar{a}^{-1}\bar{\boldsymbol{u}}_{m,h}, \bar{\boldsymbol{\varphi}}_{\boldsymbol{u}})_\Omega - (\nabla\cdot\bar{\boldsymbol{u}}_{m,h}, \bar{\varphi}_p)_\Omega \\
&\quad \pm (\bar{a}^{-1}\bar{\boldsymbol{u}}_{m,h}, \bar{\boldsymbol{\varphi}}_{\boldsymbol{u}})_{\Omega,Q} \qquad \text{[by (13)]} \\
&= (f, \bar{\varphi}_p)_\Omega - \langle g, \bar{\boldsymbol{\varphi}}_{\boldsymbol{u}}\cdot\boldsymbol{n}\rangle_{\partial\Omega} + (\bar{p}_{m,h}, \nabla\cdot\bar{\boldsymbol{\varphi}}_{\boldsymbol{u}})_\Omega - (\bar{a}^{-1}\bar{\boldsymbol{u}}_{m,h}, \bar{\boldsymbol{\varphi}}_{\boldsymbol{u}})_{\Omega,Q} - (\nabla\cdot\bar{\boldsymbol{u}}_{m,h}, \bar{\varphi}_p)_\Omega \\
&\quad + QE1(\bar{\boldsymbol{\varphi}}_{\boldsymbol{u}}) \pm (\bar{a}_m^{-1}\bar{\boldsymbol{u}}_{m,h}, \bar{\boldsymbol{\varphi}}_{\boldsymbol{u}})_{\Omega,Q} \\
&= (f, \bar{\varphi}_p)_\Omega - \langle g, \bar{\boldsymbol{\varphi}}_{\boldsymbol{u}}\cdot\boldsymbol{n}\rangle_{\partial\Omega} + (\bar{p}_{m,h}, \nabla\cdot\bar{\boldsymbol{\varphi}}_{\boldsymbol{u}})_\Omega - (\bar{a}_m^{-1}\bar{\boldsymbol{u}}_{m,h}, \bar{\boldsymbol{\varphi}}_{\boldsymbol{u}})_{\Omega,Q} - (\nabla\cdot\bar{\boldsymbol{u}}_{m,h}, \bar{\varphi}_p)_\Omega \\
&\quad + QE1(\bar{\boldsymbol{\varphi}}_{\boldsymbol{u}}) + \left((\bar{a}_m^{-1} - \bar{a}^{-1})\bar{\boldsymbol{u}}_{m,h}, \bar{\boldsymbol{\varphi}}_{\boldsymbol{u}}\right)_{\Omega,Q}.
\end{aligned} \tag{20}$$

The remaining terms are obtained by the use of (14) and (15), i.e., by Galerkin orthogonality.

□

Equation (18) represents a minor improvement to the error representation formula presented in [14]. Since the forward solution and therefore the error $\bar{e}_p$ depends upon the value of $\bar{a}_m$ at the quadrature points alone, we have modified the representation formula so that all integrals involving $\bar{a}_m$ are evaluated using the appropriate quadrature.

4.2 Error estimation for sample interface problems

We derive an error representation formula for each sample problem (10) by representing the error in the quantity of interest as the sum of the error due to the approximation of the nominal problem and the error due to the difference between the nominal and sample solutions. In order to calculate the contribution due to the difference between the nominal and sample solutions, we require the solution to the adjoint problem associated with the discretized model nominal problem: Find $(\bar{\varphi}_{p,h}, \bar{\boldsymbol{\varphi}}_{\boldsymbol{u},h}) \in W_h \times \boldsymbol{V}_h$ such that

$$\begin{aligned}
(\bar{a}_m^{-1}\bar{\boldsymbol{\varphi}}_{\boldsymbol{u},h}, \boldsymbol{v}_h)_{\Omega,Q} + (\bar{\varphi}_{p,h}, \nabla\cdot\boldsymbol{v}_h)_\Omega = 0 \quad \forall\, \boldsymbol{v}_h \in \boldsymbol{V}_h, \\
-(\nabla\cdot\bar{\boldsymbol{\varphi}}_{\boldsymbol{u},h}, w_h)_\Omega = (\psi, w_h)_\Omega \quad \forall\, w_h \in W_h.
\end{aligned} \tag{21}$$

Using the solution to (21), we obtain the following error representation formula for each sample interface problem.

Theorem 4.2. **`[Error estimate for a sample interface problem]`**
Let $(p_{m,h}^{(n)}, \boldsymbol{u}_{m,h}^{(n)})$ be the solution of (16) and $(\bar{\varphi}_{p,h}, \bar{\boldsymbol{\varphi}}_{\boldsymbol{u},h})$ satisfy the adjoint problem (21). The total error $e_p^{(n)} = \bar{p} - p_{m,h}^{(n)}$ is the sum of the nominal error $\bar{e}_p = \bar{p} - \bar{p}_{m,h}$ (see Theorem 4.1) and the sample error $e_{p,n} = \bar{p}_{m,h} - p_{m,h}^{(n)}$, i.e.,

$$(e_p^{(n)}, \psi) = \underbrace{(\bar{e}_p, \psi)}_{\text{nominal error}} + \underbrace{\left(a_m^{(n)^{-1}} - \bar{a}_m^{-1})\boldsymbol{u}_{m,h}^{(n)}, \bar{\boldsymbol{\varphi}}_{\boldsymbol{u},h}\right)_{\Omega,Q}}_{\text{sample error}}. \tag{22}$$

Proof. Adding and subtracting $(\bar{p}_{m,h}, \psi)$,

$$\left(\bar{p} - p_{m,h}^{(n)}, \psi\right)_\Omega = \left((\bar{p} - \bar{p}_{m,h}) + (\bar{p}_{m,h} - p_{m,h}^{(n)}), \psi\right)_\Omega = (\bar{e}_p, \psi)_\Omega + \left(\bar{p}_{m,h} - p_{m,h}^{(n)}, \psi\right)_\Omega. \tag{23}$$

The first term is obtained from Theorem 4.1. The second term depends on the difference between the nominal and

sample interfaces. Using the adjoint solution $(\bar{\varphi}_p, \bar{\boldsymbol{\varphi}}_{\boldsymbol{u},h})$, we obtain from (21) and integration by parts,

$$
\begin{aligned}
&(p^{(n)}_{m,h} - \bar{p}_{m,h}, \psi) \\
&\quad = -(p^{(n)}_{m,h} - \bar{p}_{m,h}, \nabla \cdot \bar{\boldsymbol{\varphi}}_{\boldsymbol{u},h})_\Omega \\
&\qquad + (\bar{a}_m^{-1}(\boldsymbol{u}^{(n)}_{m,h} - \bar{\boldsymbol{u}}_{m,h}), \bar{\boldsymbol{\varphi}}_{\boldsymbol{u},h})_{\Omega,Q} + (\bar{\varphi}_{p,h}, \nabla \cdot (\boldsymbol{u}^{(n)}_{m,h} - \bar{\boldsymbol{u}}_{m,h}))_\Omega \\
&\quad = (\bar{a}_m^{-1}\boldsymbol{u}^{(n)}_{m,h}, \bar{\boldsymbol{\varphi}}_{\boldsymbol{u},h})_{\Omega,Q} - (p^{(n)}_{m,h}, \nabla \cdot \bar{\boldsymbol{\varphi}}_{\boldsymbol{u},h})_\Omega - (\bar{a}_m^{-1}\bar{\boldsymbol{u}}_{m,h}, \bar{\boldsymbol{\varphi}}_{\boldsymbol{u},h})_{\Omega,Q} + (\bar{p}_{m,h}, \nabla \cdot \bar{\boldsymbol{\varphi}}_{\boldsymbol{u},h})_\Omega \\
&\qquad + (\bar{\varphi}_{p,h}, \nabla \cdot (\boldsymbol{u}^{(n)}_{m,h} - \bar{\boldsymbol{u}}_{m,h}))_\Omega \\
&\quad = (\bar{a}_m^{-1}\boldsymbol{u}^{(n)}_{m,h}, \bar{\boldsymbol{\varphi}}_{\boldsymbol{u},h})_{\Omega,Q} - (p^{(n)}_{m,h}, \nabla \cdot \bar{\boldsymbol{\varphi}}_{\boldsymbol{u},h})_\Omega + \langle g, \bar{\boldsymbol{\varphi}}_{\boldsymbol{u},h} \cdot \boldsymbol{n} \rangle_{\partial\Omega,M} \\
&\qquad + (\nabla \cdot (\boldsymbol{u}^{(n)}_{m,h} - \bar{\boldsymbol{u}}_{m,h}), \bar{\varphi}_{p,h})_\Omega \qquad \text{[by (14)(a)]} \\
&\quad = (\bar{a}_m^{-1}\boldsymbol{u}^{(n)}_{m,h}, \bar{\boldsymbol{\varphi}}_{\boldsymbol{u},h})_{\Omega,Q} - (p^{(n)}_{m,h}, \nabla \cdot \bar{\boldsymbol{\varphi}}_{\boldsymbol{u},h})_\Omega + \langle g, \bar{\boldsymbol{\varphi}}_{\boldsymbol{u},h} \cdot \boldsymbol{n} \rangle_{\partial\Omega,M} \\
&\qquad \pm (a^{(n)\,-1}_m \boldsymbol{u}^{(n)}_{m,h}, \bar{\boldsymbol{\varphi}}_{\boldsymbol{u},h})_{\Omega,Q} \qquad \text{[by (14)(b) and (16)(b)]} \\
&\quad = \langle g, \bar{\boldsymbol{\varphi}}_{\boldsymbol{u},h} \cdot \boldsymbol{n} \rangle_{\partial\Omega,M} + (a^{(n)\,-1}_m \boldsymbol{u}^{(n)}_{m,h}, \bar{\boldsymbol{\varphi}}_{\boldsymbol{u},h})_{\Omega,Q} - (p^{(n)}_{m,h}, \nabla \cdot \bar{\boldsymbol{\varphi}}_{\boldsymbol{u},h})_\Omega \\
&\qquad + \big((\bar{a}_m^{-1} - a^{(n)\,-1}_m)\boldsymbol{u}^{(n)}_{m,h}, \bar{\boldsymbol{\varphi}}_{\boldsymbol{u},h}\big)_{\Omega,Q} \qquad \text{[by (16)(a)]} \\
&\quad = \big((\bar{a}_m^{-1} - a^{(n)\,-1}_m)\boldsymbol{u}^{(n)}_{m,h}, \bar{\boldsymbol{\varphi}}_{\boldsymbol{u},h}\big)_{\Omega,Q}.
\end{aligned}
\tag{24}
$$

□

Note that the adjoint solution appearing in the second term of Theorem 4.2 is $\bar{\boldsymbol{\varphi}}_{\boldsymbol{u},h}$ which depends on the nominal problem and is independent of the particular sample problem. The result for a general linear operator is given in Appendix A.

While it does not require adjoint solutions to each sample problem, Theorem 4.2 does require the approximate solution to the sample problem, $\boldsymbol{u}^{(n)}_{m,h}$. If the cumulative distribution function for the quantity of interest is sought, then this is not an issue since the solution to each sample problem is required. Further, the fact that the modeling domains for the nominal problem and the sample problem should be close together can also be used to advantage. Denote the modeling domain for the nominal interface and the sample interface by $\bar{\Omega}_d$ and $\Omega^{(n)}_d$ respectively. The mass matrix to solve for the sample problem is equal to the mass matrix for the nominal problem, outside of the region $\Omega_d = \bar{\Omega}_d \cup \Omega^{(n)}_d$ since the diffusivity coefficients for the two problems are equal outside of this region. This saves a considerable amount of cost assembling the mass matrix for each problem.

However there are situations in which a cheap estimate of the cumulative distribution function for the *errors* in the quantity of interest would be useful, even in the absence of the cumulative distribution function for the quantity of interest itself. A cumulative distribution function for the errors in the quantity of interest could provide, for example, a confidence bound for the error in the quantity of interest for any particular sample. Based on the following lemma, an approximate error bound can be constructed given an assumption that every sample interface lies close to the nominal interface.

Lemma 4.1. [Approximation of the sample error]
Let $\bar{\boldsymbol{u}}_{m,h}$ and $\boldsymbol{u}^{(n)}_{m,h}$ satisfy (14) and (16) respectively and $\|\cdot\|_{\Omega,Q}$ be the norm generated by the discrete inner product $\langle \cdot, \cdot \rangle_{\Omega,Q}$. Then,

$$
\begin{aligned}
&\big((\bar{a}_m^{-1} - a^{(n)\,-1}_m)\boldsymbol{u}^{(n)}_{m,h}, \bar{\boldsymbol{\varphi}}_{\boldsymbol{u},h}\big)_{\Omega,Q} = \\
&\qquad \big((\bar{a}_m^{-1} - a^{(n)\,-1}_m)\bar{\boldsymbol{u}}_{m,h}, \bar{\boldsymbol{\varphi}}_{\boldsymbol{u},h}\big)_{\Omega,Q} + \mathcal{O}(\|\bar{a}_m^{-1} - a^{(n)\,-1}_m\|^2_{\Omega,Q}).
\end{aligned}
\tag{25}
$$

Proof. First we write the left side of (25) as

$$\begin{aligned}\big((\bar{a}_m^{-1} - {a_m^{(n)}}^{-1})\boldsymbol{u}_{m,h}^{(n)}, \bar{\boldsymbol{\varphi}}_{\boldsymbol{u},h}\big)_{\Omega,Q} = \\ \big((\bar{a}_m^{-1} - {a_m^{(n)}}^{-1})\bar{\boldsymbol{u}}_{m,h}, \bar{\boldsymbol{\varphi}}_{\boldsymbol{u},h}\big)_{\Omega,Q} + \big((\bar{a}_m^{-1} - {a_m^{(n)}}^{-1})(\boldsymbol{u}_{m,h}^{(n)} - \bar{\boldsymbol{u}}_{m,h}), \bar{\boldsymbol{\varphi}}_{\boldsymbol{u},h}\big)_{\Omega,Q}.\end{aligned} \tag{26}$$

We apply a similar strategy to that found in [14] to the second term on the right hand side. Subtracting (16) from (14) we obtain,

$$\begin{aligned}(\bar{a}_m^{-1}\bar{\boldsymbol{u}}_{m,h} - {a_m^{(n)}}^{-1}\boldsymbol{u}_{m,h}^{(n)}, \boldsymbol{v}_h)_{\Omega,Q} - (\bar{p}_{m,h} - p_{m,h}^{(n)}, \nabla\cdot\boldsymbol{v}_h)_\Omega = 0 \qquad \forall\, \boldsymbol{v}_h \in \boldsymbol{V}_h, \\ (\nabla\cdot(\bar{\boldsymbol{u}}_{m,h} - \boldsymbol{u}_{m,h}^{(n)}), w_h)_\Omega = 0 \qquad \forall\, w_h \in W_h.\end{aligned} \tag{27}$$

Choosing $\boldsymbol{v}_h = \bar{\boldsymbol{u}}_{m,h} - \boldsymbol{u}_{m,h}^{(n)}$ and $w_h = \bar{p}_{m,h} - p_{m,h}^{(n)}$, (27) simplifies to become

$$\big(\bar{a}_m^{-1}(\bar{\boldsymbol{u}}_{m,h} - \boldsymbol{u}_{m,h}^{(n)}), \bar{\boldsymbol{u}}_{m,h} - \boldsymbol{u}_{m,h}^{(n)}\big)_{\Omega,Q} = \big((\bar{a}_m^{-1} - {a_m^{(n)}}^{-1})\boldsymbol{u}_{m,h}^{(n)}, \bar{\boldsymbol{u}}_{m,h} - \boldsymbol{u}_{m,h}^{(n)}\big)_{\Omega,Q}. \tag{28}$$

Taking the norm of both sides we obtain,

$$\|\bar{\boldsymbol{u}}_{m,h} - \boldsymbol{u}_{m,h}^{(n)}\|_{\Omega,Q} \le C\|\bar{a}_m^{-1} - {a_m^{(n)}}^{-1}\|_{\Omega,Q}. \tag{29}$$

Therefore,

$$\big((\bar{a}_m^{-1} - {a_m^{(n)}}^{-1})(\boldsymbol{u}_{m,h}^{(n)} - \bar{\boldsymbol{u}}_{m,h}), \bar{\boldsymbol{\varphi}}_{\boldsymbol{u},h}\big)_{\Omega,Q} = \mathcal{O}(\|\bar{a}_m^{-1} - {a_m^{(n)}}^{-1}\|_{\Omega,Q}^2). \tag{30}$$

□

Lemma 4.1 shows that we can replace $\boldsymbol{u}_{m,h}^{(n)}$ in Theorem 4.2 with $\bar{\boldsymbol{u}}_{m,h}$ by ignoring a higher order term and therefore, under these circumstances, it is unnecessary to solve the forward problem for each sample problem in order to compute the error in each sample problem. The computation for the error representation formula can be further simplified by noting that $\bar{a}_m^{-1} - {a_m^{(n)}}^{-1}$ is zero outside of Ω_d, the modeling domain. We arrive at the following approximate error representation formula.

Theorem 4.3. [Approximate error estimate for a sample interface problem]
Let $(\bar{p}_{m,h}, \bar{\boldsymbol{u}}_{m,h})$ be the solution of (14) and $(\bar{\varphi}_{p,h}, \bar{\boldsymbol{\varphi}}_{\boldsymbol{u},h})$ satisfy (21). If $\|\bar{a}_m^{-1} - {a_m^{(n)}}^{-1}\|_{\Omega,Q}^2$ is small compared to $\big((\bar{a}_m^{-1} - {a_m^{(n)}}^{-1})\bar{\boldsymbol{u}}_{m,h}, \bar{\boldsymbol{\varphi}}_{\boldsymbol{u},h}\big)_{\Omega,Q}$, then

$$(e_p^{(n)}, \psi) = \underbrace{(\bar{e}_p, \psi)}_{\text{nominal error}} + \underbrace{\big(({a_m^{(n)}}^{-1} - \bar{a}_m^{-1})\bar{\boldsymbol{u}}_{m,h}, \bar{\boldsymbol{\varphi}}_{\boldsymbol{u},h}\big)_{\Omega_d,Q}}_{\text{approximate sample error}}. \tag{31}$$

Proof. Follows directly from Theorem 4.2 and Lemma 4.1. □

The computational cost of evaluating the error representation in Theorem 4.3 is small since we must only evaluate the second term at the quadrature nodes within the modeling domain.

5. NUMERICAL EXAMPLES

We first present numerical examples that demonstrate the accuracy of the error representation formula in Theorem 4.3 for individual sample problems. We then use Theorem 4.3 to approximate the cumulative distribution function (cdf) for the error in the quantity of interest and assess the accuracy of our approximate cdf. Finally we examine the conditions for which Theorems 4.2 and 4.3 are applicable.

For each of the examples below, the following computational parameters are used unless otherwise stated. Our domain is given by $\Omega = [0,1]\times[0,1]$ and we discretize uniformly in both the x and y directions with a grid size of

$h = \frac{1}{8}$ to solve the forward problem. To solve the adjoint problem we discretize uniformly with a grid size of $\frac{h}{2}$. Both the forward and adjoint problems are solved using the MFEC method outlined in Section 3. The quantity of interest is chosen to be the average of the solution over the domain.

We define the true interface Γ to be the zero level set of a function $\gamma(x, y)$. The diffusivity coefficient is constant on either side of the interface,

$$a(x,y) = \begin{cases} a^+, & \gamma(x,y) > 0, \\ a^-, & \gamma(x,y) \leq 0, \end{cases} \tag{32}$$

where $a^+ = 1$ and $a^- = 10$. The boundary term g is identically zero and the forcing term f is a function of $\gamma(x, y)$ and is chosen such that the exact solution is

$$p(x,y) = \begin{cases} \dfrac{1}{a^+}\, x(x-1)\, y(y-1)\, \gamma(x,y), & \gamma(x,y) > 0, \\ \dfrac{1}{a^-}\, x(x-1)\, y(y-1)\, \gamma(x,y), & \gamma(x,y) \leq 0. \end{cases} \tag{33}$$

The exact solution is therefore continuous across the true interface Γ.

We simulate experimental measurements of the interface location and use those measurement to construct a spline that approximates the location of the interface as described in Section 2.1. For each sample interface $\Gamma^{(n)}$, we obtain $P = 10$ uniformly spaced points $(x_i, y_i)_{i=1}^P$ from the true interface Γ. The coordinates of these points are perturbed by adding independent normally distributed random error resulting in "measurements" given by

$$\begin{aligned} x_i^{(n)} &= x_i + \epsilon_{i,x}^{(n)}, \\ y_i^{(n)} &= y_i + \epsilon_{i,y}^{(n)}, \end{aligned} \tag{34}$$

where $\epsilon_{i,x}^{(n)}$ and $\epsilon_{i,y}^{(n)}$ are sampled from a normal distribution with zero mean and variance σ^2.

The effectivity ratio

$$\mathcal{E} = \frac{\text{Estimated Error}}{\text{Exact Error}},$$

is used to measure the accuracy of the error estimator. The more accurate the error estimate, the closer $\mathcal{E}$ is to one. We plot the difference between the effectivity ratio and one, i.e., $|1 - \mathcal{E}|$ in order to more clearly demonstrate our results.

Exact integration of the coefficient $\bar{a}^{-1}$ is required in the error representation formula. Since these coefficient are discontinuous, typical Gaussian quadrature does not suffice and we use the midpoint rule on a highly refined mesh within the cut cells.

5.1 Error estimation using Theorem 4.3

We begin by demonstrating the approximate sample error representation formula in Theorem (4.3) for sample interfaces near the nominal interface. In §5.1.1 we simulate measuring the radius of a circle with true radius r. This generates a one parameter family of sample interfaces, each of which is a circle with a measured radius $r^{(n)}$. In §5.1.2 we simulate measurements on the boundary of a circle and construct a spline approximation to the circle as explained above.

5.1.1 Measurements of the radius of a circle

The true interface of a circle centered at (x_0, y_0) with radius r is given as the zero level set of the function

$$\gamma(x,y) = (x - x_0)^2 + (y - y_0)^2 - r^2.$$

For the true interface Γ, we use a circle centered at $(0.5, 0.51)$ with radius $r = 0.32$. For simplicity, we choose the nominal interface $\bar{\Gamma} = \Gamma$ for this example. The sample interfaces $\Gamma^{(n)}$ are obtained by simulating measurements of the radius of a circle. Therefore, each sample interface is a circle centered at $(0.5, 0.51)$ with radius $r^{(n)}$ given by

$$r^{(n)} = r + \epsilon^{(n)} \text{ with } \epsilon^{(n)} \sim \mathcal{N}(0, 0.1).$$

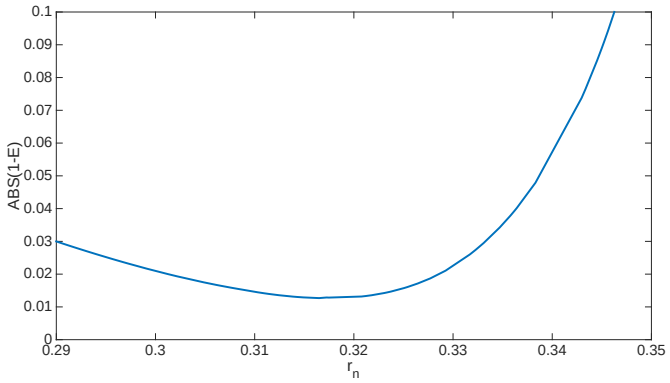

FIG. 2: Difference between the effectivity ratio of the error estimate and one, $|1 - \mathcal{E}|$, for the interface problem for 50 measurements of the radius of the circle.

In this example the forcing function $f^{(n)}$ is defined differently for each sample problem and is determined using (33). This requires an extra term in the error representation formula equal to

$$(f^{(n)} - \bar{f}, \bar{\varphi}_p)_\Omega - (f^{(n)} - \bar{f}, \bar{\varphi}_{p,h})_{\Omega, M_x M_y},$$

which represents the difference in source terms $\bar{f}$ and $f^{(n)}$ for the nominal and sample problems respectively.

Figure 2 shows the difference between the effectivity ratio and the ideal value of one. Note that the near the radius of the nominal circle ($r = 0.32$), the error estimator performs well. However the accuracy of the error estimator decreases as the difference between the sample and nominal interfaces increases.

5.1.2 Measurements of the boundary of a circle

In this example we simulate measurements of the boundary of the circle at $P = 10$ locations as described above and using a value of $\sigma^2 = 0.01$. An exact solution is not available for the nominal problem and we approximate an exact solution with $\bar{p}_{\text{exact}}$ using a highly refined approximation. To calculate $\bar{p}_{\text{exact}}$ we discretize the grid uniformly with a grid size $h = \frac{1}{64}$, and use the MFEC method to solve (11).

Figure 3 shows the difference between the effectivity ratio and the ideal value of one for 50 samples of the measured circle. Noting the scale, we observe that the effectivity ratio is close to one for all samples.

5.1.3 Assessing the range of applicability of Theorem 4.3

We now consider an interface that is defined as the zero level set of

$$\gamma(x, y) = 8(x - 0.09)(x^2 - 0.29)(x^2 - 0.75)(x - 1.2) - y + 0.55. \tag{35}$$

This interface is shown in Figure 4. Note that this interface is qualitatively different from the circle in two ways. Firstly, it is not a closed curve and enters the domain at one boundary and leaves at another. Secondly, there are two changes in concavity for this interface whereas the circle has no changes in concavity.

We use this example to consider the effect of the variance of the measurements on the error. We start with a variance of $\sigma^2 = 0.01$ and increase it to $\sigma^2 = 0.2$. For each value of the variance, we estimate the error for $N = 50$ samples and also calculate the exact error for those same sample interfaces in order to calculate an effectivity ratio. Table 1 shows the average error in the effectivity ratios for the error representation formulas presented in both Theorem 4.2 and Theorem 4.3. If Theorem 4.3 is used, the accuracy of the error estimator decreases as the uncertainty in the

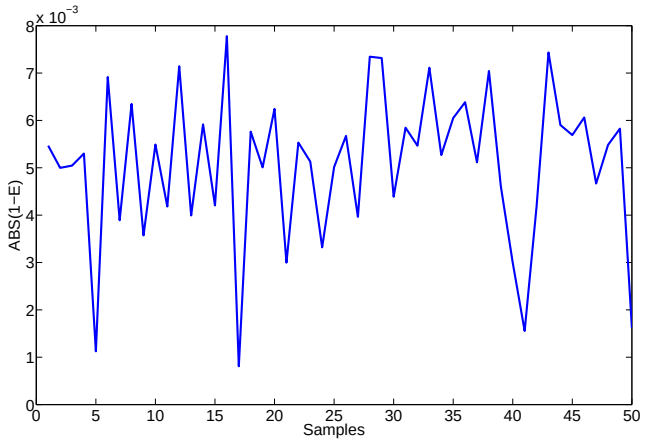

FIG. 3: Difference between the effectivity ratio of the error estimate and one, $|1 - \mathcal{E}|$, for the interface problem for 50 sets of measurements of the boundary of the circle at $P = 10$ locations.

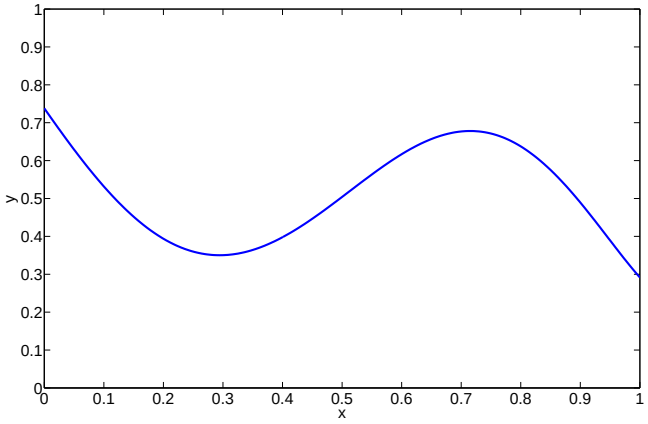

FIG. 4: The exact polynomial interface for $\gamma(x, y)$ given by (35).

σ^2	**Thm. 4.2**	**Thm. 4.3**
0.01	1.43e-02	2.75e-02
0.05	1.58e-02	1.48e-01
0.1	4.79e-02	1.57e+00
0.2	2.91e-02	1.93e+00

TABLE 1: Mean of the difference between the effectivity ratio of the error estimate and one, $|1 - \mathcal{E}|$, for different values of the variance in the measurement error using Theorems 4.2 and 4.3.

measurements increases. The error estimator is consistently accurate for all values of the variance if Theorem 4.2 is used.

It would be useful to have a method of determining *a priori* when the approximate error representation formula in Theorem 4.3 can be used, and when the uncertainty is too large and Theorem 4.2 must be used. There is currently no analytical method of determining this, however if both error estimates are computed for a small number of sample problems, their results can be compared. If the error estimates are similar, it can be reasonably assumed that the approximate error formula is appropriate to use. However, if the two error estimates are very different, than the exact error representation formula should be used to ensure accurate calculations.

5.2 The cumulative distribution function for the error using Theorem 4.3

To approximate the cumulative distribution function for the error in a quantity of interest, we use Theorem 4.3 to estimate the error in the quantity of interest for N sample interfaces. These error estimates $\mathcal{Q}(e^{(n)}),\ n = 1, \ldots, N$ are used to approximate the cumulative distribution function using the estimator

$$F_N(t) = \frac{1}{N} \sum_{i=1}^{N} I(\mathcal{Q}(e^{(n)}) \leq t), \tag{36}$$

where I is the indicator function. To approximate the exact cumulative distribution function $F(t)$, we approximate the exact error as described in Section 5.1.2 for a large number of samples $N_{\text{exact}} \gg N$ and use the estimator (36).

5.2.1 Measurements of the boundary of a circle

We revisit the circle example with the same forcing function and discretization and choose a variance of $\sigma^2 = 0.01$. To approximate the cumulative distribution function we use $N = 200$ samples. Since the exact cumulative distribution function is unknown, a higher quality approximation to the exact cumulative distribution function is computed using $\bar{p}_{\text{exact}}$ and $N_{\text{exact}} = 2000$ samples.

The "exact" and approximate cumulative distribution functions are shown in Figure 5. In Table 2, we measure the accuracy of our approximate cumulative distribution function using $\mathcal{E}_\mu$ and $\mathcal{E}_{\sigma^2}$, defined by

$$\mathcal{E}_\mu = \frac{\text{Mean of } F_N(t)}{\text{Mean of } F(t)}, \quad \mathcal{E}_{\sigma^2} = \frac{\text{Variance of } F_N(t)}{\text{Variance of } F(t)},$$

which indicate how accurately the mean and variance of $F(t)$ is estimated by $F_N(t)$. For accurate estimators, these ratios would be near unity. We observe that the mean is well estimated, but the variance is not. This is largely due to the relatively small number of samples which result in the exact cumulative distribution functions having longer tails than the approximate cumulative distribution functions.

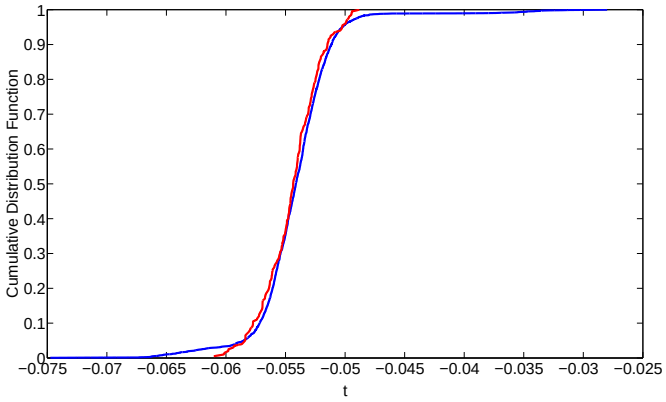

FIG. 5: "Exact" and approximate cumulative distribution function for the errors in the quantity of interest using Theorem 4.3 for 200 sets of measurements of the boundary of the circle at $P = 10$ locations.

Interface	$\mathcal{E}_{\mu}$	$\mathcal{E}_{\sigma^2}$
Circle	1.00e+00	4.65e-01
Polynomial	1.00e+00	9.78e-01

TABLE 2: Effectivity ratios for the mean and variance of the cumulative distribution function for two interfaces.

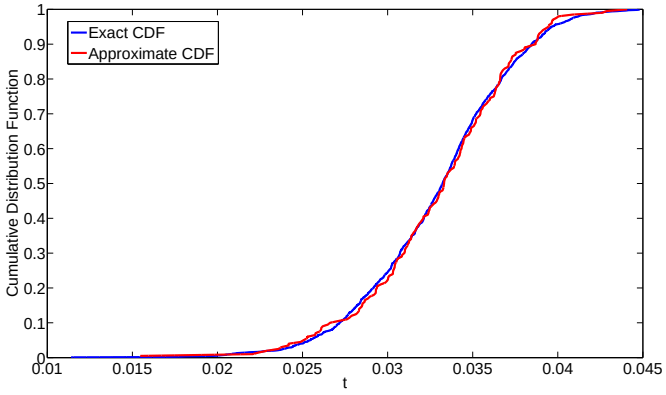

FIG. 6: "Exact" and approximate cumulative distribution functions for the errors in the quantity of interest using Theorem 4.3 for 200 sets of measurements of the polynomial interface at $P = 10$ locations.

5.2.2 Measurements from the polynomial interface

Here, the measurements are uniformly distributed across the interface and are perturbed by a Gaussian distribution with zero mean and variance $\sigma^2 = 0.01$. We approximate the cumulative distribution function using $N = 200$ samples. An exact solution to the nominal problem is obtained with a grid size of $h = \frac{1}{64}$ and $F(t)$ is computed using $N_{\text{exact}} = 2000$ samples. The exact and approximate cumulative distribution function lie very close to each other as

seen in Figure 6 and from Table 2 we see that in this example both the mean and variance of the error are estimated well by the approximate cumulative distribution function.

5.3 Nominal error vs sample error

Finally we consider the competing effects of the discretization size h and the variance of the measurement error σ^2 on each of the nominal and sample errors and on the total error. If we refine the discretization grid, but use the same value for the variance of the measurement error, eventually the measurement error will dominate. At this point, more accurate measurements are needed to decrease the total error. Conversely, if we have a fixed discretizetion and decrease the variance of the measurement error, eventually the discretization error will dominate. For the following results, we use the polynomial interface.

5.3.1 Grid refinement with a fixed variance for the measurement error

We fix the variance of the error in the measurements at $\sigma^2 = 0.03$ and consider grid sizes of $h = \frac{1}{8}, \frac{1}{16}$, and $\frac{1}{32}$. For each of these grid parameters, we estimate the error using Theorem 4.3 for $N = 200$ samples. The nominal error, the expectation of the sample error and the expectation of the total error are shown in Table 3. Obviously as h decreases, the nominal error decreases since the nominal error depends on the discretization. The measurement error however is essentially independent of the mesh size, i.e., remains constant as the grid is refined since it depends only on the difference between the sample problem and the nominal problem. For coarse discretizations, the nominal error dominates, but as the grid is refined, the measurement error eventually comes to dominate. Beyond this point, the total error stops decreasing and there is no advantage to further refining the grid. Instead, to reduce the error we must obtain more accurate measurements.

h	**E(|Total|)**	**|Nominal|**	**E(|Sample|)**	**Ratio**
1/4	7.29e-02	6.97e-02	1.08e-02	0.15
1/8	3.38e-02	3.58e-02	7.63e-03	0.21
1/16	1.00e-02	9.19e-03	8.01e-03	0.87
1/32	8.09e-03	2.30e-03	7.88e-03	3.42

TABLE 3: The expectation of the absolute value of the total error, the absolute value of the nominal error, and the expectation of the absolute value of the sample error for $N = 200$ samples using Theorem 4.3. The ratio is the expectation of the absolute value of the sample error to the absolute value of the nominal error.

5.3.2 Increasing the variance of the measurement error with a fixed mesh

We now use Theorem 4.2 to estimate the error components for a fixed mesh size as the variance of the measurement error is increased. The results for $N = 200$ samples are shown in Table 4. We see that the error in the nominal solution remains essentially unchanged, while the sample error increases as σ^2 increases. As expected, the change in σ^2 does not effect the approximation error since the nominal interface will change only very slightly for each different value of σ, However, σ^2 does affect the expectation of the absolute error in the sample interfaces. For small variance, the nominal error dominates the sample errors and the total error remains relatively constant, but as the variance in the sample interfaces increases, the measurement error begins to dominate and the total error increases.

6. CONCLUSIONS

We have derived an efficient adjoint-based *a posteriori* error estimation formula for a diffusive process with an interface whose location is defined by a relatively small number of experimental measurements, each of which is subject to error. We assume the errors in the experimental measurements can be modelled by a Gaussian distribution and

σ^2	E(|Total|)	|Nominal|	E(|Sample|)	Ratio
0.01	3.29e-02	3.43e-02	3.54e-03	0.10
0.05	3.01e-02	3.31e-02	1.28e-02	0.39
0.1	2.87e-02	3.30e-02	2.75e-02	0.83
0.2	4.46e-02	3.48e-02	5.56e-02	1.6
0.5	1.08e-01	2.90e-02	1.23e-01	4.2

TABLE 4: The expectation of the absolute value of the total error, the absolute value of the nominal error, and the expectation of the absolute value of the sample error for $N = 200$ samples using Theorem 4.3. The ratio is the expectation of the absolute value of the sample error to the absolute value of the nominal error.

construct spline approximations through realizations of the interface locations. We approximate the unknown true interface with a "nominal" interface and compute the error of our numerical solution to this nominal problem. We then compute the error for each sample interface problem as the error of the nominal problem plus a term that depends upon the difference between the nominal and sample problems. By comparing the relative sizes of the nominal and sample errors we can determine how to best decrease the error in our approximation, either via grid refinement or by reducing the measurement errors.

ACKNOWLEDGMENTS

This research was supported by the Computational Mathematics program of the National Science Foundation under grant DMS-1016268. D. Estep's work is supported in part by the Defense Threat Reduction Agency (HDTRA1-09-1-0036), Department of Energy (DE-FG02-04ER25620, DE-FG02-05ER25699, DE-FC02-07ER54909, DE-SC0001724, DE-SC0005304, INL00120133), Idaho National Laboratory (00069249, 00115474), Lawrence Livermore National Laboratory (B584647, B590495), National Science Foundation (DMS-0107832, DMS-0715135, DGE-0221595003, MSPA-CSE-0434354, ECCS-0700559, DMS-1065046, DMS-1016268, DMS-FRG-1065046), National Institutes of Health (#R01GM096192).

APPENDIX A. THE GENERAL (LINEAR) CASE

We develop the analogues of Theorems 4.2 and 4.3 for general linear operators.

APPENDIX A.1 The continuous problem

(This is the "nominal" problem in §2.3, i.e., our approximation to the true operator.)

Forward problem: Find $\bar{u} \in U$ such that

$$(\bar{L}\bar{u}, v) = (f, v) \; \forall v \in V, \tag{A.1}$$

where $\bar{L} : U \mapsto V^*$ and $f \in V^*$.

Adjoint operator: Define $\bar{L}^*$ such that

$$(\bar{L}u, v) = (u, \bar{L}^* v) \; \forall u \in U, v \in V, \tag{A.2}$$

where $\bar{L} : U \mapsto V^*$ and $\bar{L}^* : V \mapsto U^*$.

Adjoint problem: Find $\phi \in V$ such that

$$(w, \bar{L}^*\phi) = (w, \psi) \; \forall w \in U, \tag{A.3}$$

where $\psi \in U^*$.

Error estimation: Given an approximate solution $u_h \in U_h \subset U$, let $e = \bar{u} - u_h \in U$. For $\psi \in U^*$,

$$(e, \psi) = (e, \bar{L}^* \phi) = (\bar{L} e, \phi) = (\bar{L}\bar{u} - \bar{L} u_h, \phi). \tag{A.4}$$

Since $\phi \in V$, add zero in the form $(f, \phi) - (\bar{L}\bar{u}, \phi)$ to give

$$(e, \psi) = (f - \bar{L} u_h, \phi) := (R, \phi). \tag{A.5}$$

APPENDIX A.2 The discretized problem

A discrete approximation to the continuous nominal problem.

Discrete forward problem: Find $\bar{u}_h \in U_h \subset U$ such that

$$(\bar{L}_h \bar{u}_h, v_h) = (f, v_h) \; \forall v_h \in V_h \subset V. \tag{A.6}$$

Define

$$\bar{e} = \bar{u} - \bar{u}_h. \tag{A.7}$$

Discrete adjoint operator Define $\bar{L}_h^*$ such that

$$(\bar{L}_h u_h, v_h) = (u_h, \bar{L}_h^* v_h) \; \forall u_h \in U_h, v_h \in V_h, \tag{A.8}$$

where $\bar{L}_h : U_h \mapsto V_h^*$ and $\bar{L}_h^* : V_h \mapsto U_h^*$.

Discrete adjoint problem Find $\phi_h \in V_h$ such that

$$(w_h, \bar{L}_h^* \phi_h) = (w_h, \psi) \; \forall w_h \in U_h \subset U, \tag{A.9}$$

where $\psi \in U^*$.

APPENDIX A.3 Discrete sample problems

Given N discrete sample problems and N discrete operators $L_h^{(n)}, n = 1, \ldots, N$.

Discrete sample forward problem: Find $u_h^{(n)} \in U_h \subset U$ such that

$$(L_h^{(n)} u_h^{(n)}, v_h) = (f, v_h) \; \forall v_h \in V_h \subset V, \tag{A.10}$$

where $L_h^{(n)} : U_h \mapsto V_h^*$.

Error estimation for discrete sample problems: Let

$$e^{(n)} = \bar{u} - u_h^{(n)} = (\bar{u} - \bar{u}_h) + (\bar{u}_h - u_h^{(n)}) = \bar{e} + (u_h - u_h^{(n)}) \in U \tag{A.11}$$

hence

$$\begin{aligned}
(e^{(n)}, \psi) &= (\bar{e}, \psi) + (\bar{u}_h - u_h^{(n)}, \psi) \\
&= (\bar{e}, \psi) + (\bar{u}_h - u_h^{(n)}, \bar{L}_h^* \phi_h) \\
&= (\bar{e}, \psi) + (\bar{L}_h(\bar{u}_h - u_h^{(n)}), \phi_h) \\
&= (\bar{e}, \psi) + (\bar{L}_h(\bar{u}_h - u_h^{(n)}), \phi_h) \pm (L_h^{(n)} u_h^{(n)}, \phi_h) \\
&= (\bar{e}, \psi) + (\bar{L}_h \bar{u}_h - L_h^{(n)} u_h^{(n)}, \phi_h) + ((L_h^{(n)} - \bar{L}_h) u_h^{(n)}, \phi_h) \\
&= (\bar{e}, \psi) + ((L_h^{(n)} - \bar{L}_h) u_h^{(n)}, \phi_h),
\end{aligned} \tag{A.12}$$

with the final simplification from (A.6) and (A.10) noting $\phi_h \in V_h$.

Note: If the right hand sides in (A.6) and (A.10) are f_h and $f_h^{(n)}$ respectively, there is an extra term of the form $(f_h - f_h^{(n)}, \phi_h)$ in (A.12).

If, further, it can be shown that

$$((L_h^{(n)} - \bar{L}_h)(\bar{u}_h - u_h^{(n)}), \phi_h), \tag{A.13}$$

is higher order, then

$$(e^{(n)}, \psi) = (\bar{e}, \psi) + ((L_h^{(n)} - \bar{L}_h)\bar{u}_h, \phi_h). \tag{A.14}$$

REFERENCES

1. Estep, D., Målqvist, A., and Tavener, S., Nonparametric density estimation for randomly perturbed elliptic problems I: Computational methods, a posteriori analysis, and adaptive error control, *SIAM Journal on Scientific Computing*, 31(4):2935–2959, 2009.
2. Oden, J. T., Babuska, I., Nobile, F., Feng, Y., and Tempone, R., Theory and methodology for estimation and control of errors due to modeling, approximation, and uncertainty, *Computer Methods in Applied Mechanics and Engineering*, 194:195–204, 2005.
3. Liang, B. and Mahadevan, S., Error and uncertainty quantification and sensitivity analysis in mechanics computational models, *International Journal for Uncertainty Quantification*, 1(2):147–161, 2011.
4. Aziz, K. and Settari, A., *Petroleum reservoir simulation*, Vol. 476, Applied Science Publishers London, 1979.
5. Cancès, C., Gallouët, T., and Porretta, A., Two-phase flows involving capillary barriers in heterogeneous porous media, *arXiv preprint arXiv:1005.5634*, 2010.
6. Van Duijn, C., Molenaar, J., and De Neef, M., The effect of capillary forces on immiscible two-phase flow in heterogeneous porous media, *Transport in Porous Media*, 21(1):71–93, 1995.
7. Jou, H.-J., Leo, P. H., and Lowengrub, J. S., Microstructural evolution in inhomogeneous elastic media, *Journal of Computational Physics*, 131(1):109–148, 1997.
8. Lin, T., Sheen, D., and Zhang, X., A locking-free immersed finite element method for planar elasticity interface problems, *Journal of Computational Physics*, 247:228–247, 2013.
9. Sigmund, O., Design of multiphysics actuators using topology optimization–part II: Two-material structures, *Computer Methods in Applied Mechanics and Engineering*, 190:6605–6627, 2001.
10. Wiegmann, A. and Zemitis, A., *EJ-HEAT: A fast explicit jump harmonic averaging solver for the effective heat conductivity of composite materials*, Fraunhofer-Institut für Techno-und Wirtschaftsmathematik, Fraunhofer (ITWM), 2006.
11. Ramirez, J., Stan, M., and Cristea, P., Simulations of heat and oxygen diffusion in UO_2 nuclear fuel rods, *Journal of Nuclear Materials*, 359(3):174–184, 2006.
12. Newman, C., Hansen, G., and Gaston, D., Three dimensional coupled simulation of thermomechanics, heat, and oxygen diffusion in UO_2 nuclear fuel rods, *Journal of Nuclear Materials*, 392(1):6–15, 2009.
13. Williamson, R., Hales, J., Novascone, S., Tonks, M., Gaston, D., Permann, C., Andrs, D., and Martineau, R., Multidimensional multiphysics simulation of nuclear fuel behavior, *Journal of Nuclear Materials*, 423(1):149–163, 2012.
14. Wang, H., Pernice, M., Tavener, S., and Estep, D., A posteriori error analysis for a cut cell finite volume method, *Computer Methods in Applied Mechanics and Engineering*, 200(INL/JOU-09-17376), 2011.
15. Frank, T., Tertois, A.-L., and Mallet, J.-L., 3d-reconstruction of complex geological interfaces from irregularly distributed and noisy point data, *Computers & Geosciences*, 33(7):932–943, 2007.

16. Neuman, S. P. and Orr, S., Prediction of steady state flow in nonuniform geological media by conditional moments: Exact nonlocal formalism, effective conductivities, and weak approximation, *Water Resources Research*, 29(2):341–364, 1993.

17. Neuman, S., Tartakovsky, D., Wallstrom, T., and Winter, C., Correction to "Prediction of steady state flow in nonuniform geological media by conditional moments: Exact nonlocal formalism, effective conductivities, and weak approximation", by Shlomo P. Neuman and Shlomo Orr, *Water Resources Research*, 32(5):1479–1480, 1996.

18. Barajas-Solano, D. A. and Tartakovsky, D. M., Computing Green's functions for flow in a heterogeneous composite media, *International Journal for Uncertainty Quantification*, 3(1):39–46, 2013.

19. Ruppert, D., Wand, M. P., and Carroll, R. J., *Semiparametric Regression*, Cambridge University Press, 2003.

20. Arbogast, T., Wheeler, M. F., and Yotov, I., Mixed finite elements for elliptic problems with tensor coefficients as cell-centered finite differences, *SIAM Journal on Numerical Analysis*, 34(2):828–852, 1997.

21. Brezzi, F. and Fortin, M., *Mixed and hybrid finite element methods*, Springer-Verlag New York, Inc., 1991.

22. Estep, D., Pernice, M., Pham, D., Tavener, S., and Wang, H., A posteriori error analysis of a cell-centered finite volume method for semilinear elliptic problems, *Journal of Computational and Applied Mathematics*, 233(2):459–472, 2009.